Dental Materials Journal 2017; 36(4): 482–490

Effects of experimental pastes containing surface pre-reacted glass ionomer fillers on inhibition of enamel demineralization

Keiki NAKAMURA[1], Hidenori HAMBA[1,2], Syozi NAKASHIMA[1], Alireza SADR[3], Toru NIKAIDO[1], Masakazu OIKAWA[4], Motohiro UO[5] and Junji TAGAMI[1]

[1] *Department of Cariology and Operative Dentistry, Division of Oral Health Sciences, Graduate School of Medical and Dental Science, Tokyo Medical and Dental University (TMDU), Tokyo, Japan*
[2] *Department of Endodontics and Clinical Cariology, Tokyo Dental College, Tokyo, Japan*
[3] *Department of Restorative Dentistry, University of Washington School of Dentistry, Seattle, WA, United States*
[4] *National Institute of Radiological Sciences, National Institute for Quantum and Radiological Science and Technology, Chiba, Japan*
[5] *Department of Advanced Biomaterials, Division of Oral Health Sciences, Graduate School of Medical and Dental Science, Tokyo Medical and Dental University (TMDU), Tokyo, Japan*
Corresponding author, Hidenori HAMBA; E-mail: hamba.ope@gmail.com

This study aimed to evaluate the inhibitory effect of experimental pastes containing surface pre-reacted glass ionomer (S-PRG) fillers on enamel demineralization. Bovine blocks were treated twice a day for 4 days by 7 groups; experimental pastes containing 0–30 wt% S-PRG filler (S00, S01, S05, S10, and S30), deionized water (DW) as negative control, and NaF paste (MP) as positive control. The surfaces were demineralized by acetic acid for 3 days. Mineral loss (ML) was calculated by micro-computed X-ray tomography. The treated surface was finally investigated with scanning electron microscope (SEM) and micro-focused particle induced X-ray emission (micro-PIXE). S05, S10 and S30 demonstrated significantly lower ML than S00, S01 and DW ($p<0.05$). S10 showed the greatest inhibitory effect, which was significantly greater than MP. The S-PRG filler containing experimental pastes demonstrated a potential to inhibit enamel demineralization. Sr ion incorporation was confirmed on the enamel surface with the experimental pastes.

Keywords: Demineralization, Enamel, Micro-CT, Micro-PIXE, S-PRG filler

INTRODUCTION

Regular brushing with fluoride containing experimental paste can lower the rate of dental caries incidence[1,2]. Topical applications of fluoride gel and varnish are also well established as therapeutic agents, providing protection against acid challenges as well as repair of demineralized enamel[3-5]. Fluoride has been shown to reduce enamel mineral loss following acid erosion challenges *via in-vitro* and *in-situ* studies[2,6,7].

Recently, surface pre-reacted glass ionomer (S-PRG) filler has been developed, which is composed of fluoroboroaliminosilicate glass and polyacrylic acid solution and is produced through acid-base reaction[8]. The S-PRG filler has been incorporated into resinous materials, such as dentin bonding agents[9,10], fissure sealants[11,12], and resin composites[13]. The S-PRG containing resinous materials can release multiple ions, such as aluminium (Al), boron (B), fluoride (F), sodium (Na), silicon (Si), and strontium (Sr), in neutral and acidic conditions[14]. It was reported that among the ions released from the S-PRG fillers, Sr had the highest amount, followed by F and Si[14].

Micro-computed X-ray tomography (micro-CT) can capture three-dimensional (3D) architectural information from samples non-destructively[15]. The technique has been shown as a promising method to assess demineralization or remineralization of enamel or dentin[16-19]. The use of micro-CT has been validated for quantitative assessment of enamel demineralization[20].

Particle induced X-ray emission (PIXE) analysis uses the characteristic X-rays generated by accelerated proton (or a charged particle) to detect elements. By focusing the incident beam down to micron size and scanning over the specimen surface, "micro-PIXE" can also provide images of the trace elemental distribution with high spatial resolution (μm scale) and high sensitivity[21,22]. The method has been used to analyze the distribution of trace heavy elements contained in various soft and hard tissues[23-26].

The purpose of this study was to evaluate the inhibitory effects of experimental pastes containing S-PRG fillers on bovine enamel demineralization using micro-CT, scanning electron microscope (SEM) and micro-PIXE. The null hypothesis was that the experimental pastes could not prevent enamel demineralization when subjected to acid challenge.

MATERIALS AND METHODS

Specimen preparation

Twenty extracted, non-damaged permanent bovine incisors were stored frozen until the experiment. The teeth were thoroughly cleaned and washed under running water to remove all adherent soft tissues. The specimens were prepared by cutting into 3×3×2 mm enamel-dentin blocks using a low-speed diamond saw (Isomet, Buehler, Lake Bluff, IL, USA) under

Color figures can be viewed in the online issue, which is available at J-STAGE.

Received Sep 5, 2016: Accepted Dec 19, 2016
doi:10.4012/dmj.2016-303 JOI JST.JSTAGE/dmj/2016-303

water as a coolant. The enamel surfaces were ground flat with 600- to 2000-grit silicon carbide (SiC) papers (Fuji Star, Sankyo Rikagaku, Saitama, Japan) under running water. The surfaces were then covered by a nail varnish (680, Revlon, New York, NY, USA) leaving a window (2×2 mm) to expose the polished enamel surface of each specimen. In order to set a reference landmark for the micro-CT scans, a hole (1 mm in diameter, 0.5 mm in depth) was made at the side of the specimen by a diamond bur (440SS ISO # 010, Shofu, Kyoto, Japan). They were then divided into seven treatment groups to give a total of 70 specimens listed in Table 1; deionized water (Direct-Q, Millipore, Billerica, MA, USA) (DW) as a negative control, 950 ppm F (as NaF) commercially available paste (Merssage Plus, Shofu) (MP) as a positive control and experimental pastes containing 0, 1, 5, 10, and 30 wt% of S-PRG fillers (Shofu) (S00, S01, S05, S10, and S30, respectively). Experimental paste suspensions were prepared at dilution of 1:2 (paste: deionized water), thoroughly stirred and mechanically agitated for 1 min by means of a vortex mixer (MF-71, TGK, Tokyo, Japan) according to the procedures described in the previous study[27]. The specimens were immersed in each suspension at 37°C for 5 min twice a day, rinsed off using deionized water for 10 s and returned to the storage in deionized water in the incubator at 37°C. The treatment cycle continued for 4 days, and the suspensions were prepared daily. After the treatment cycle was completed, the specimens were scanned by micro-CT to establish a baseline. Each specimen was then separately immersed in 10 mL of a demineralizing solution (2.2 mM $CaCl_2$, 2.2 mM KH_2PO_4 and 50 mM acetic acid adjusted at pH 4.5 with 10 M KOH) at 37°C for 3 days[28]. The demineralizing solution was refreshed daily. After the demineralization, the specimens were removed from the solution and scanned by micro-CT again (Fig. 1).

Micro-CT scanning

A micro-CT system (InspeXio SMX-100CT, Shimadzu, Kyoto, Japan) was used to evaluate mineral density (MD) of the demineralized specimens. The micro-CT system can generate polychromatic X-rays with cone-beam geometry. A 0.2-mm thick brass (Cu-Zn) filter was installed in the beam path to reduce beam-hardening effect[19,29] . The specimen was mounted on a computer-controlled turntable, which synchronized the rotation and the axial shift. The nominal isotropic resolution of the setup was 8.1 μm with an integration time of 120 s. The scanning was performed with the specimen being rotated 360° at rotation step of 0.6°. The tube voltage was 100 kV at a current of 120 μA. The distance from X-ray source to the sample was 39.2 mm, and that from X-ray source to the detector was 300 mm. The specimen was mounted so that the X-ray beam was perpendicular to the treated enamel surface.

For MD calibration, a series of mineral reference phantoms were also scanned which included three hydroxyapatite (HAp) disks in total (Ratoc, Tokyo, Japan); two with different concentrations (0.50 and 0.70 gHAp/cm^3) of HAp crystals embedded in epoxy resin (Epoxicure Resin, Buehler), and one pure HAp disk (3.16 gHAp/cm^3) (Cellyard, Hoya, Tokyo, Japan).

Micro-CT image analysis

The data in each scan were acquired as 100 images in 16-bit TIFF format, and used to reconstruct a 3D image stack from the 2D images, with a resolution of 512×512 pixels and an isotropic volumetric pixel (voxel) size of 8.1 μm by a 3D analysis software (TRI/3D-BON, Ratoc), which was used for visualization and quantitative volumetric measurements. CT values were converted into MD values (gHAp/cm^3) using a linear calibration curve based on the grey values obtained from the mineral reference phantoms (linear regression, R^2>0.9994). A noise reducing median filter was applied to the data,

Table 1 Materials used in this study

Group	Product	Ingredients		Lot	Manufacturer
		S-PRG filler	Others		
S00	Experimental paste	0 wt%	Sorbit liquid, Anhydrous silicic acid, Glycerin, Carboxymethyl cellulose, Purified water, *etc.*	081101	Shofu, Kyoto, Japan
S01		1 wt%		081101	
S05		5 wt%		081101	
S10		10 wt%		081101	
S30		30 wt%		081101	
MP	Merssage plus	Silicic acid, Glycerin, Carboxymethyl cellulose, Pyrophosphoric acid, 950 ppm F as NaF, Chlorhexidine hydrochloride, Purified water, *etc.*		PN0575	
DW	Direct-Q	Deionized water		—	Millipore, Billerica, MA, US

S-PRG: Surface reaction-type of pre-reacted glassionomer, NaF: Sodium fluoride

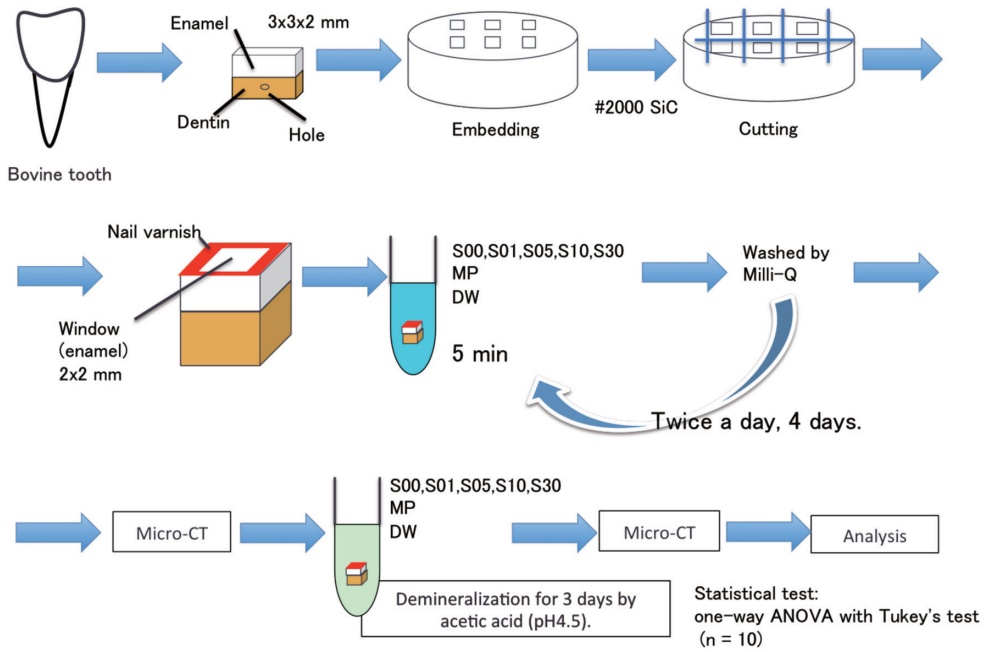

Fig. 1 Schematic representation of specimen preparation and scanning by micro-CT.

and the background was removed by excluding those pixels with a CT value lower than the zero MD value according to the calibration curve. The rendered 3D volumes were manually translated and rotated in the software to visually match the baseline image, which served as the reference. The features on each image used for the matching process were the sound enamel surface, specimen edges and reference landmarks (holes made by a bur on dentin). The assessment was performed in a volume of interest (VOI) of 486×486×486 μm^3 at the center of the demineralization window. Mean MD values were calculated in the VOI at each 8.1 µm depth. The MD profile in each specimen was obtained by plotting the mineral density (vol%). All maximum MD in baseline (sound) specimen was normalized to 100 vol% against the depth.

Mean integrated mineral loss (ML) (vol% µm) after each demineralization period was calculated from the MD profiles; with the reference point of the depth axis (0 µm) set at the axial position of the sound enamel surface at baseline. The ML on each specimen was calculated from the MD profiles by subtracting the area under the curve after demineralization from the area before demineralization as shown in Fig. 2. These calculations were performed by importing the MD data for each depth of demineralization into spread sheet software package (Microsoft Excel for Windows version 2013, Microsoft, Redmond, WA, USA).

SEM observation

Specimens were prepared in the same manner as for micro-CT observation. Morphology of enamel surface at the treatment window was observed by SEM

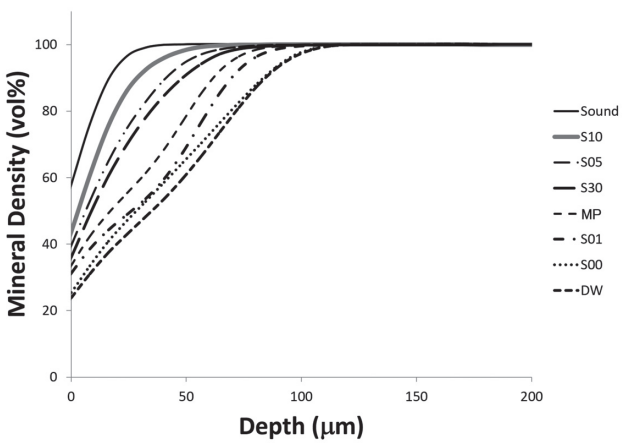

Fig. 2 Mean MD profiles for each experimental group. Graphs show the mean mineral density profiles with the distance in x-axis (µm) and relative mineral content (%) in y-axis, before the demineralization (sound) and after 3-day demineralization in the DW, S00, S01, MP, S30, S05, and S10 groups.

(JSM-5310LV, JEOL, Tokyo, Japan) under ×3,500 magnification on extra specimens in each group before and after demineralization, following a specimen processing protocol for SEM, which included desiccation and gold sputter coating.

Micro-PIXE observation

Additional specimens from the S10 and DW groups (before and after demineralization) were subjected to

the micro-PIXE analysis. The specimens were cut into 0.5×3×2 mm enamel-dentin slices at the center of the treatment window using a low-speed diamond saw (Isomet) under water as a coolant. The cross-sectional surface was then ground flat with 2000-grit aluminum oxide carbide papers (Lapping paper, 3M ESPE, St. Paul, MN, USA) under running water for observation.

Micro-PIXE analyses were conducted at the National Institute of Radiological Sciences (Chiba, Japan). An accelerated and micro-focused proton beam (3.0 MeV, 2 μm beam diameter) with raster scanning was applied over the target area of the specimen (maximum area of 2×2 mm) on two surfaces; on the demineralized enamel surface (imaging from top) and on the polished cross-section. The generated characteristic X-rays were collected using Si (Li) and CdTe detectors to obtain the elemental distribution images and the characteristic X-ray spectra. The obtained data were processed with analysis software (OMDAQ2007, Oxford Microbeams, Bicester, UK), and the elemental distribution images were obtained.

Statistical analysis

The ML results were expressed as mean and standard deviation. The collected values were statistically analyzed using one-way ANOVA with Tukey's test. The significance level of all tests was set at α=0.05. All statistical tests were performed with a computerized statistical program (SPSS for Windows Ver. 11, SPSS, Chicago, IL, USA).

RESULTS

Micro-CT analysis

A typical 2D image of the control group after demineralization was shown in Fig. 3. The DW group revealed approximately 100 μm thickness of demineralized enamel.

Mean mineral density profiles

The MD profiles of enamel in each experimental group were summarized in Fig. 2. After demineralization, the DW group revealed the most aggressive mineral loss pattern among all the groups. In the S00 and S01 groups, the profiles showed patterns similar to that of the DW group. The S05 and S30 groups showed mineral profiles similar to each other, representing less mineral loss compared to the DW group. On the other hand, the S10 group showed the least mineral loss among all the treatment groups. In the MP group, the profile showed an intermediate pattern between the S30 and DW groups.

Mean mineral loss

The mean ML value of each group was summarized in Fig. 4. The highest ML value was obtained in the S00, S01, and DW groups, which were not significantly different each other (p>0.05). The S05, S10 and S30 groups showed significantly less ML than the S00, S01 and DW groups (p<0.05). In terms of nominal values, S10 was the most effective in inhibition of enamel demineralization, followed by S05 and S30, however, there was no statistically significant difference among them (p>0.05). The MP group showed significantly larger mineral loss compared to the S10 group (p<0.05); there was no significant difference between MP and any other groups (p>0.05).

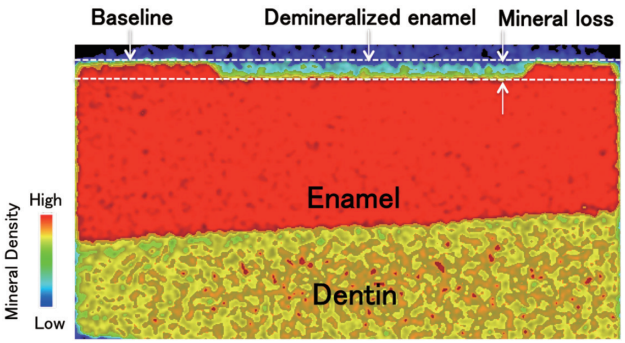

Fig. 3 Micro-CT 2D image of a specimen in control group showing sound enamel surface (as baseline) and demineralized lesion for measurement of MD through enamel surface in a VOI of 461×461×461 μm at the center of the treated surface.

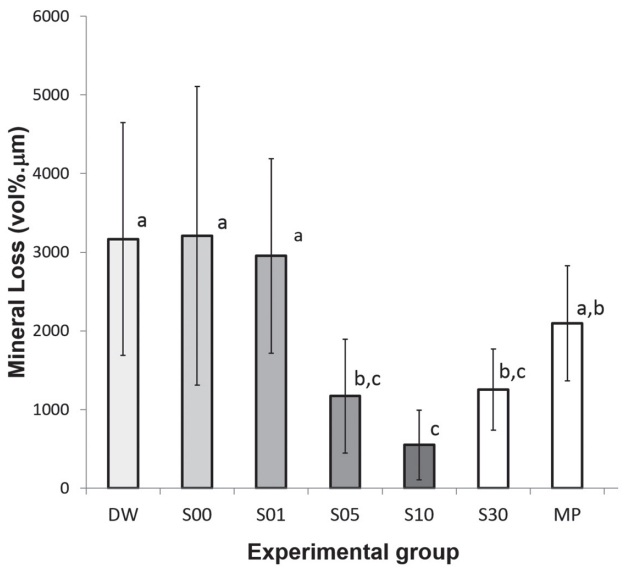

Fig. 4 Mean ML (vol%・μm) for each experimental group. Results are expressed as means and standard deviations (SD). Similar lower case letters indicate no significant difference amongst the values (p>0.05).

SEM observation

The representative SEM micrographs of the enamel surfaces before and after demineralization are shown in Fig. 5. The smear layer covering the enamel surface was visible after the treatment cycle and before demineralization in all the groups. After the

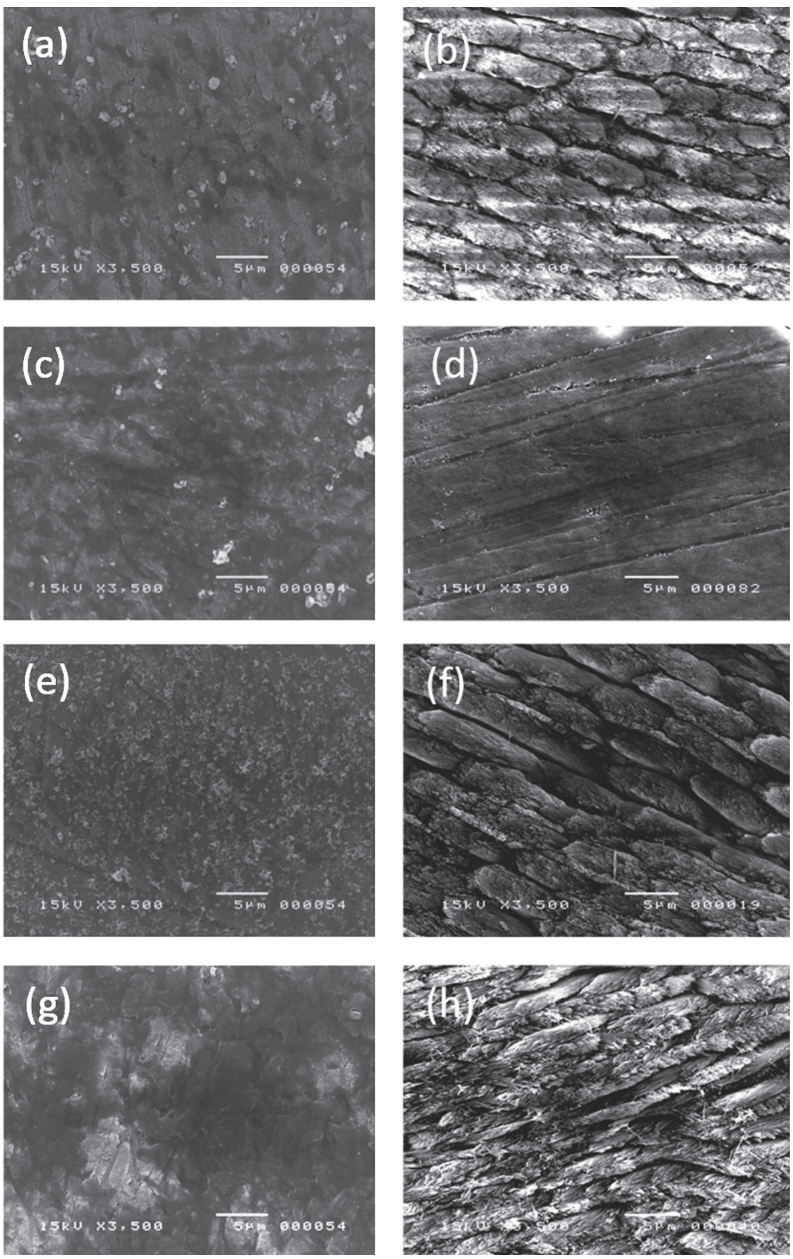

Fig. 5 SEM micrographs of enamel surface treated with the paste S00 (a), S10 (c), MP (e), groups and DW (g) groups before demineralization.
S00 (b), S10 (d), MP (f), and DW (h) groups after demineralization. The residues of the experimental pastes were remained on the enamel surfaces in S00, S10, and MP groups. The smear layers resulting from SiC paper polishing were observed on the enamel surface in DW group (g). The honey-comb like structures were observed in S00, MP and DW groups. The surface texture of S00 and DW groups were more distinct compared with that of MP group. The smear layer was removed, but a smoother surface was observed in S10 group. The scratches are created by SiC paper polishing.

demineralization, the prismatic enamel structures were exposed in the S00 (Fig. 5b), MP (Fig. 5f), and DW (Fig. 5h) groups. However, the enamel prism structures were not observed after demineralization in the S10 group (Fig. 5d), while the smear layer was removed and distinct scratches (due to SiC polishing) were observed.

Micro-PIXE observation

The elemental distribution images of Ca and Sr on the enamel surfaces after the treatment in the DW and S10 groups obtained by the micro-PIXE analysis are shown in Fig. 6. In both specimen, Ca was homogeneously distributed on enamel surface and no difference could be

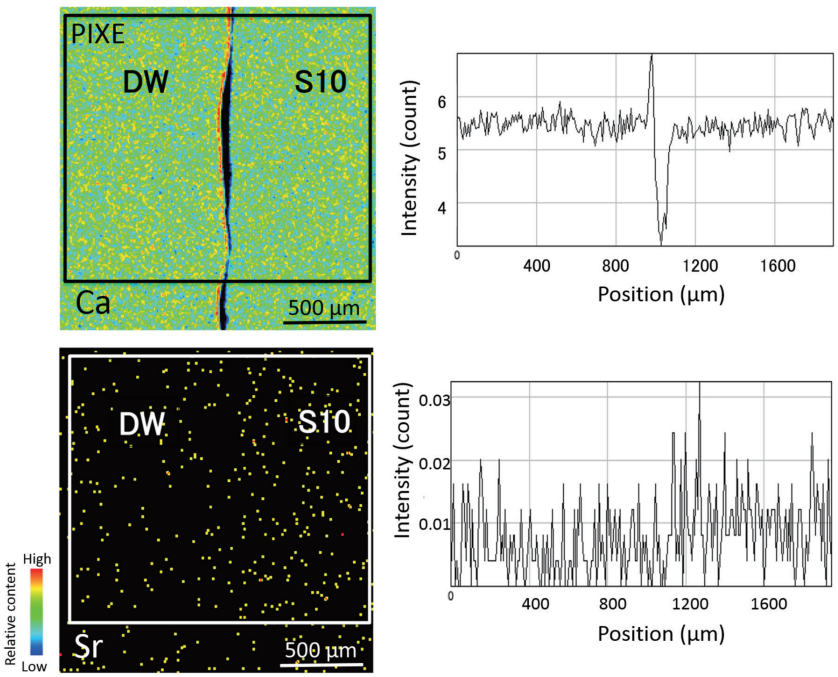

Fig. 6 Elemental distribution of Ca and Sr on the surface of DW and S10 treated groups obtained by micro-PIXE.
The two specimens were placed next to each other and scanned to facilitate direct comparison. Ca distribution on the enamel surface was similar between DW and S10 groups. On the other hand, elemental concentration of Sr on surface of S10 group was slightly higher than that of DW group. The line profiles correspond to cumulative distribution of each element through the square area of interest.

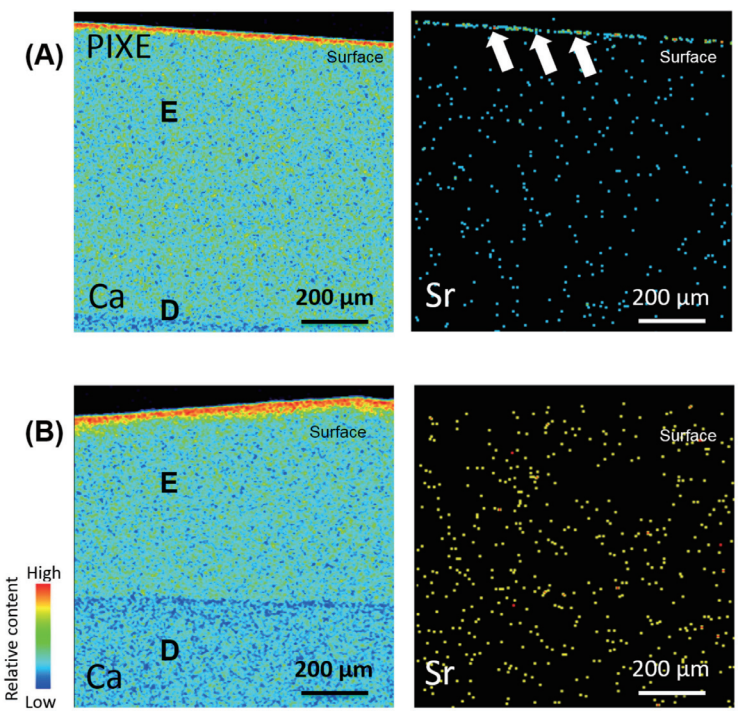

Fig. 7 Elemental distribution images of Ca and Sr of the cross-section obtained after S10 treatments (A) and after demineralization (B).
E: enamel, D: dentin. Sr adsorption on the enamel surface was clearly obtained after S10 treatment (white arrows in A), but not after demineralization (B).

observed between the DW and S10 groups. In contrast, Sr could be detected on enamel surface in the S10 group, but not in the DW group. Figure 7 depicts the representative distribution images of Ca and Sr on the cross section of enamel surface in the specimen of the S10 group before and after demineralization (Figs. 7A and B, respectively). Ca distribution through the cross-section of enamel was similar distribution before and after the demineralization. Sr accumulation was detected on the enamel surface after the S10 treatment; however, the accumulated Sr on the enamel surface disappeared after demineralization.

DISCUSSION

Micro-CT is a powerful research tool that yields 3D information about hard tissues, allowing dynamic detection of mineral change after demineralization and remineralization of enamel and dentin. Micro-CT can be used as a nondestructive alternative to the 'gold standard' method of transverse microradiography, with comparable parameters for the study of mineral content and lesion depth. In addition, its accuracy can be increased by reducing beam-hardening effects and using appropriate mineral density calibration curves[20].

Experimental pastes are daily oral care products to prevent caries, periodontal disease, or acid erosion. Experimental pastes are recognized as the best source of fluoride, which are the most effective treatment to protect both deciduous and permanent teeth from caries. Fluoride concentration in the whole saliva is related to the efficiency of caries prevention and experimental pastes are normally diluted in the process of brushing[30]; therefore, the experimental pastes used in this study were diluted three times with distilled water. The suspensions were used to simulate oral situation.

The effect of different concentrations of the S-PRG fillers in the experimental pastes on inhibition of enamel demineralization was evaluated in this study. Concentrations of the S-PRG fillers in the experimental paste ranged from 0 to 30 wt% in the experiment. A commercially available fluoride paste containing 950 ppm F (MP) was used as a positive control.

According to the MD profiles of the micro-CT assessment, inhibition of the enamel demineralization was variable in the different groups (Fig. 2). As expected the MD profile of the negative control (DW) group indicated the most aggressive demineralization of enamel. The experimental pastes containing 5 wt% or more S-PRG demonstrated significantly lower ML values than the negative control group. In addition, S10 was the only group, which was more effective than the positive control, commercially available fluoride paste in inhibiting demineralization. Viscosity of the S30 group was harder than the other experimental pastes in our pilot study. Previous study reported enamel loss was dependent on viscosity of acid[31]. High viscosity decreased the ion exchange and clearance of dissolution products. High viscosity of the S30 group suggested a prevention of ion exchange on tooth surface at a slow rate.

The representative SEM micrographs indicated different features of enamel surfaces among the groups (Fig. 5). The protective effects of S10 against demineralization were evident from the SEM images, where the typical honeycomb etching pattern of enamel was absent unlike other groups in which enamel surface was clearly demineralized (Figs. 5c and d). These findings are in line with the micro-CT results.

The S-PRG filler particles are produced by acid-base reaction of fluoroboroaluminosilicate glass and polyacrylic acid, which is known to have a potential to release multi-ions including Al, B, Na, Si, Sr, and F[14]. Fujimoto *et al.* measured concentration of F ions released from the S-PRG filler in distilled water using inductively coupled plasma atomic emission spectroscopy (ICP-AES) and fluoride ion electrode methods. They reported that up to 90 ppm of fluoride ions were detected from the slurry of the S-PRG fillers with distilled water[14], which was smaller F concentration than expected from the glass ionomer filler. This fact suggests that the effect of inhibition of demineralization of the S-PRG filler containing experimental pastes was not only due to F ions, but also related to other ions released from the S-PRG fillers[32]. A recent study on a S-PRG containing coating material also suggested that multiple ions release from these fillers increased the resistance of enamel against demineralization[33]. It was shown that ions released from the S-PRG filler had antibacterial and pH neutralizing effects on acidic solutions[34-36].

In a previous study, over 250 ppm of ionized Sr was detected from a suspension of the S-PRG fillers diluted twice with water[13]. Dedhiya *et al.* reported that Ca-Sr apatite complex could form at the apatite crystal surface in presence of Sr ions, which may play an important role in retardation of acid dissolution[37]. Sr is a homologous element of Ca which is thought to promote mineralization in conjunction with F[8,38-40].

Therefore, micro-PIXE analysis was done in the current study to detect Sr on the enamel surface. Micro-PIXE detects multi-elemental distribution in biological samples with high spatial resolution (1 μm range) and high sensitivity (down to μg/g range)[41]. According to the surface analysis of enamel using micro-PIXE, intensity of Ca was similar between the DW and S10 groups, while intensity of Sr was higher in the S10 group than in the DW group (Fig. 6). In the cross-sectional enamel specimens of the S10 group, intrinsic Ca was visualized in the whole enamel area, which was almost similar before and after demineralization. On the other hands, Sr was densely absorbed on the enamel surface before demineralization, however, this phenomenon disappeared after demineralization. The accumulation of Sr on the enamel surface after immersion in the S10 suspension suggested that the inhibitory effects of the experimental paste might be explained partially by the Sr incorporation[37]. In order to reveal the mechanism of action of Sr and its interaction with enamel (*e.g.* chemical state, composition and structural changes) should be investigated in future studies.

The current study demonstrated that the S-PRG

fillers containing experimental paste could protect enamel surface from the acid attack. Further study should be carried out to evaluate the efficacy of multi-ion release from the S-PRG fillers on demineralization and remineralization of enamel and dentin.

CONCLUSIONS

Micro-CT and SEM examinations revealed that the S-PRG filler containing experimental pastes effectively inhibited demineralization of enamel surface. Micro-PIXE analysis demonstrated high concentration of Sr on the enamel surface treated with the 10 wt% S-PRG fillers containing experimental paste, suggesting that Sr may play an important role in inhibition of enamel demineralization.

ACKNOWLEDGMENTS

This work was supported by JSPS KAKENHI Grant Numbers 25870203 and by the grant from the Japanese Ministry of Education, Global Center of Excellence (GCOE) program, "International Research Center for molecular Science in Tooth and Bone Diseases". Micro-PIXE analyses were supported by the MEXT Project for Creation of Research Platforms and Sharing of Advanced Research Infrastructure (2014-001) of the National Institute of Radiological Sciences (NIRS, Japan).

CONFLICT OF INTEREST

The authors state no conflict of interest.

REFERENCES

1) Bratthall D, Hansel-Petersson G, Sundberg H. Reasons for the caries decline: what do the experts believe? Eur J Oral Sci 1996; 104: 416-422.
2) Alhawij H, Lippert F, Martinez-Mier EA. Relative fluoride response of caries lesions created in fluorotic and sound teeth studied under remineralizing conditions. J Dent 2015; 43: 103-109.
3) Malinowski M, Duggal MS, Strafford SM, Toumba KJ. The effect on dental enamel of varying concentrations of fluoridated milk with a cariogenic challenge in situ. J Dent 2012; 40: 929-933.
4) Duggal MS, Nikolopoulou A, Tahmassebi JF. The additional effect of ozone in combination with adjunct remineralisation products on inhibition of demineralisation of the dental hard tissues in situ. J Dent 2012; 40: 934-940.
5) Carvalho TS, Bonecker M, Altenburger MJ, Buzalaf MA, Sampaio FC, Lussi A. Fluoride varnishes containing calcium glycerophosphate: fluoride uptake and the effect on in vitro enamel erosion. Clin Oral Investig 2015; 19: 1429-1436.
6) Ganss C, Schulze K, Schlueter N. Toothpaste and erosion. Monogr Oral Sci 2013; 23: 88-99.
7) Bartlett DW, Smith BG, Wilson RF. Comparison of the effect of fluoride and non-fluoride toothpaste on tooth wear in vitro and the influence of enamel fluoride concentration and hardness of enamel. Br Dent J 1994; 176: 346-348.
8) Ito S, Iijima M, Hashimoto M, Tsukamoto N, Mizoguchi I, Saito T. Effects of surface pre-reacted glass-ionomer fillers on mineral induction by phosphoprotein. J Dent 2011; 39: 72-79.
9) Hotta M, Yamamoto K. Comparative radiopacity of bonding agents. J Adhes Dent 2009; 11: 207-212.
10) Iida Y, Nikaido T, Kitayama S, Takagaki T, Inoue G, Ikeda M, Foxton RM, Tagami J. Evaluation of dentin bonding performance and acid-base resistance of the interface of two-step self-etching adhesive systems. Dent Mater J 2009; 28: 493-500.
11) Han L, Okiji T. Evaluation of the ions release/incorporation of the prototype S-PRG filler-containing endodontic sealer. Dent Mater J 2011; 30: 898-903.
12) Kaga M, Kakuda S, Ida Y, Toshima H, Hashimoto M, Endo K, Sano H. Inhibition of enamel demineralization by buffering effect of S-PRG filler-containing dental sealant. Eur J Oral Sci 2014; 122: 78-83.
13) Hotta M, Morikawa T, Tamura D, Kusakabe S. Adherence of Streptococcus sanguinis and Streptococcus mutans to saliva-coated S-PRG resin blocks. Dent Mater J 2014; 33: 261-267.
14) Fujimoto Y, Iwasa M, Murayama R, Miyazaki M, Nagafuji A, Nakatsuka T. Detection of ions released from S-PRG fillers and their modulation effect. Dent Mater J 2010; 29: 392-397.
15) Elliott JC, Dover SD. X-ray microtomography. J Microsc 1982; 126: 211-213.
16) Kinney JH, Balooch M, Haupt DL, Marshall SJ, Marshall GW. Mineral distribution and dimensional changes in human dentin during demineralization. J Dent Res 1995; 74: 1179-1184.
17) Anderson P, Elliott JC, Bose U, Jones SJ. A comparison of the mineral content of enamel and dentine in human premolars and enamel pearls measured by X-ray microtomography. Arch Oral Biol 1996; 41: 281-290.
18) Songsiripradubboon S, Hamba H, Trairatvorakul C, Tagami J. Sodium fluoride mouthrinse used twice daily increased incipient caries lesion remineralization in an in situ model. J Dent 2014; 42: 271-278.
19) Hamba H, Nikaido T, Inoue G, Sadr A, Tagami J. Effects of CPP-ACP with sodium fluoride on inhibition of bovine enamel demineralization: a quantitative assessment using micro-computed tomography. J Dent 2011; 39: 405-413.
20) Hamba H, Nikaido T, Sadr A, Nakashima S, Tagami J. Enamel lesion parameter correlations between polychromatic micro-CT and TMR. J Dent Res 2012; 91: 586-591.
21) Komatsu H, Yamamoto H, Matsuda Y, Kijimura T, Kinugawa M, Okuyama K, Nomachi M, Yasuda K, Satoh T, Oikawa S. Fluorine analysis of human enamel around fluoride-containing materials under different pH-cycling by μ-PIGE/PIXE system. Nucl Instrum Methods Phys Res B 2011; 269: 2274-2277.
22) Devès G, Isaure M-P, Lay PL, Bourguignon J, Ortega R. Fully quantitative imaging of chemical elements in Arabidopsis thaliana tissues using STIM, PIXE and RBS. Nucl Instrum Methods Phys Res B 2005; 231: 117-122.
23) Sugiyama T, Uo M, Mizoguchi T, Wada T, Omagari D, Komiyama K, Mori Y. Copper accumulation in the sequestrum of medication-related osteonecrosis of the jaw. Bone Rep 2015; 3: 40-47.
24) Sugiyama T, Uo M, Wada T, Hongo T, Omagari D, Komiyama K, Sasaki H, Takahashi H, Kusama M, Mori Y. Novel metal allergy patch test using metal nanoballs. J Nanobiotechnol 2014; 12: 1-6.
25) Sugiyama T, Uo M, Wada T, Omagari D, Komiyama K, Miyazaki S, Chiya N, Noguchi T, Jinbu Y, Kusama M, Mori Y. Detection of trace metallic elements in oral lichenoid contact lesions using SR-XRF, PIXE, and XAFS. Sci Rep 2015; 5: 1-12.
26) Sugiyama T, Uo M, Wada T, Omagari D, Komiyama K, Noguchi T, Jinbu Y, Kusama M. Estimation of trace metal elements in oral mucosa specimens by using SR-XRF, PIXE, and XAFS. Biometals 2015; 28: 11-20.
27) Kumar VL, Itthagarun A, King NM. The effect of casein

phosphopeptide-amorphous calcium phosphate on remineralization of artificial caries-like lesions: an in vitro study. Aust Dent J 2008; 53: 34-40.
28) Ten Cate JM, Duijsters PP. Alternating demineralization and remineralization of artificial enamel lesions. Caries Res 1982; 16: 201-210.
29) Jennings RJ. A method for comparing beam-hardening filter materials for diagnostic radiology. Med Phys 1988; 15: 588-599.
30) Ingle NA, Sirohi R, Kaur N, Siwach A. Salivary fluoride levels after toothbrushing with dentifrices containing different concentrations of fluoride. J Int Soc Prev Community Dent 2014; 4: 129-132.
31) Aykut-Yetkiner A, Wiegand A, Bollhalder A, Becker K, Attin T. Effect of acidic solution viscosity on enamel erosion. J Dent Res 2013; 92: 289-294.
32) Murayama R, Furuichi T, Yokokawa M, Takahashi F, Kawamoto R, Takamizawa T, Kurokawa H, Miyazaki M. Ultrasonic investigation of the effect of S-PRG filler-containing coating material on bovine tooth demineralization. Dent Mater J 2012; 31: 954-959.
33) Alsayed EZ, Hariri I, Sadr A, Nakashima S, Bakhsh TA, Shimada Y, Sumi Y, Tagami J. Optical coherence tomography for evaluation of enamel and protective coatings. Dent Mater J 2015; 34: 98-107.
34) Itota T, Al-Naimi OT, Carrick TE, Yoshiyama M, McCabe JF. Fluoride release and neutralizing effect by resin-based materials. Oper Dent 2005; 30: 522-527.
35) Nicholson JW, Aggarwal A, Czarnecka B, Limanowska-Shaw H. The rate of change of pH of lactic acid exposed to glass-ionomer dental cements. Biomaterials 2000; 21: 1989-1993.
36) Wang H, Shimada Y, Tagami J. Effect of fluoride in phosphate buffer solution on bonding to artificially carious enamel. Dent Mater J 2007; 26: 722-727.
37) Dedhiya MG, Young F, Higuchi WI. Mechanism for the retardation of the acid dissolution rate of hydroxapatite by strontium. J Dent Res 1973; 52: 1097-1109.
38) Shimazu K, Ogata K, Karibe H. Evaluation of the ion-releasing and recharging abilities of a resin-based fissure sealant containing S-PRG filler. Dent Mater J 2011; 30: 923-927.
39) Featherstone JD, Shields CP, Khademazad B, Oldershaw MD. Acid reactivity of carbonated apatites with strontium and fluoride substitutions. J Dent Res 1983; 62: 1049-1053.
40) Thuy TT, Nakagaki H, Kato K, Hung PA, Inukai J, Tsuboi S, Nakagaki H, Hirose MN, Igarashi S, Robinson C. Effect of strontium in combination with fluoride on enamel remineralization in vitro. Arch Oral Biol 2008; 53: 1017-1022.
41) Schnell RM, Khodja H, Mary V, Thomine S. Using μPIXE for quantitative mapping of metal concentration in Arabidopsis thaliana seeds. Front Plant Sci 2013; 4: 1-10.